ADVANCED MATERIALS
www.advmat.de

Dopant-Free Pyrrolopyrrole-Based (PPr) Polymeric Hole-Transporting Materials for Efficient Tin-Based Perovskite Solar Cells with Stability Over 6000 h

Chun-Hsiao Kuan, Rajendiran Balasaravanan, Shih-Min Hsu, Jen-Shyang Ni, Yi-Tai Tsai, Zhong-Xiang Zhang, Ming-Chou Chen, and Eric Wei-Guang Diau**

A new set of pyrrolopyrrole-based (PPr) polymers incorporated with thioalkylated/alkylated bithiophene (SBT/BT) is synthesized and explored as hole-transporting materials (HTMs) for Sn-based perovskite solar cells (TPSCs). Three bithiophenyl spacers bearing the thioalkylated hexyl (SBT-6), thioalkylated tetradecyl (SBT-14), and tetradecyl (BT-14) chains are utilized to examine the effect of the alkyl chain lengths. Among them, the TPSCs are fabricated using PPr-SBT-14 as HTMs through a two-step approach by attaining a power conversion efficiency (PCE) of 7.6% with a remarkable long-term stability beyond 6000 h, which has not been reported elsewhere for a non-PEDOT:PSS-based TPSC. The PPr-SBT-14 device is stable under light irradiation for 5 h in air (50% relative humidity) at the maximum power point (MPP). The highly planar structure, strong intramolecular S(alkyl)···S(thiophene) interactions, and extended π-conjugation of SBT enable the PPr-SBT-14 device to outperform the standard poly(3-hexylthiophene,-2,5-diyl (P3HT) and other devices. The longer thio-tetradecyl chain in SBT-14 restricts molecular rotation and strongly affects the molecular conformation, solubility, and film wettability over other polymers. Thus, the present study makes a promising dopant-free polymeric HTM model for the future design of highly efficient and stable TPSCs.

1. Introduction

Organic–inorganic lead halide perovskites play important roles in many application fields, such as solar energy conversion,[1–6] photodetectors,[7,8] light-emitting diodes, lasers and others due to their unique optoelectronic characteristics.[9,10] Tin perovskite solar cells (TPSCs) which replace lead in the traditional B site of a perovskite structure, played a promising role for the development of lead-free PSC. Currently, TPSCs with power conversion efficiency (PCE) exceeding 14% have been reported.[11,12] However, the best-performing TPSCs were fabricated exclusively using the poly(3,4-ethylenedioxythiophene):poly(styrenesulfonate) (PEDOT:PSS) as a hole-transporting material (HTM) according to a one-step fabrication procedure because the rapid reaction between the precursors SnI_2 and FAI occurred so that the hydrophilic HTM like PEDOT:PSS was required to enhance its nucleation step. The hygroscopic character of PEDOT:PSS would degrade the device lifetime of TPSCs; therefore, finding a new HTM alternative is an urgent task to solve the stability issue of TPSCs. For example, using the hydrophobic poly[bis(4-phenyl)(2,4,6-trimethylphenyl)amine] (PTAA)[13] to replace PEDOT:PSS as an HTM has been reported for the tin perovskite layer fabricated the according to the two-step approach;[14] the self-assembled monolayer is another approach applied for TPSCs without the PEDOT:PSS as an HTM.[15]

The basic concept of designing a new HTM for TPSCs can be classified into the following four points: a) suitable highest occupied molecular orbital (HOMO)/lowest unoccupied molecular orbital (LUMO) energy levels, b) high charge mobility and conductivity, c) good solution processability, d) weak parasitic absorption, and e) good stability and low cost.[19,20] Under these considerations, polymeric HTMs have attracted considerable interest in boosting the efficiency and stability of lead-based perovskite solar cells in the past few years due to their ability to make continuous and uniform films, as well as high hole mobility with high LUMO energy levels to block electrons transferring through it. Thus, modifying of a suitable small HTM unit into a more planar polymeric framework allows a longer

C.-H. Kuan, S.-M. Hsu, E. W.-G. Diau
Department of Applied Chemistry and Institute of Molecular Science
National Yang Ming Chiao Tung University
Hsinchu 300093, Taiwan
E-mail: diau@nycu.edu.tw

R. Balasaravanan, Y.-T. Tsai, Z.-X. Zhang, M.-C. Chen
Department of Chemistry and Research Center of New Generation Light Driven Photovoltaic Modules
National Central University
Taoyuan 320317, Taiwan
E-mail: mcchen@ncu.edu.tw

J.-S. Ni
Department of Chemical and Materials Engineering
Photo-sensitive Material Advanced Research and Technology Center (Photo-SMART)
National Kaohsiung University of Science and Technology
Kaohsiung 824005, Taiwan

E. W.-G. Diau
Center for Emergent Functional Matter Science
National Yang Ming Chiao Tung University
Hsinchu 300093, Taiwan

The ORCID identification number(s) for the author(s) of this article can be found under https://doi.org/10.1002/adma.202300681

DOI: 10.1002/adma.202300681

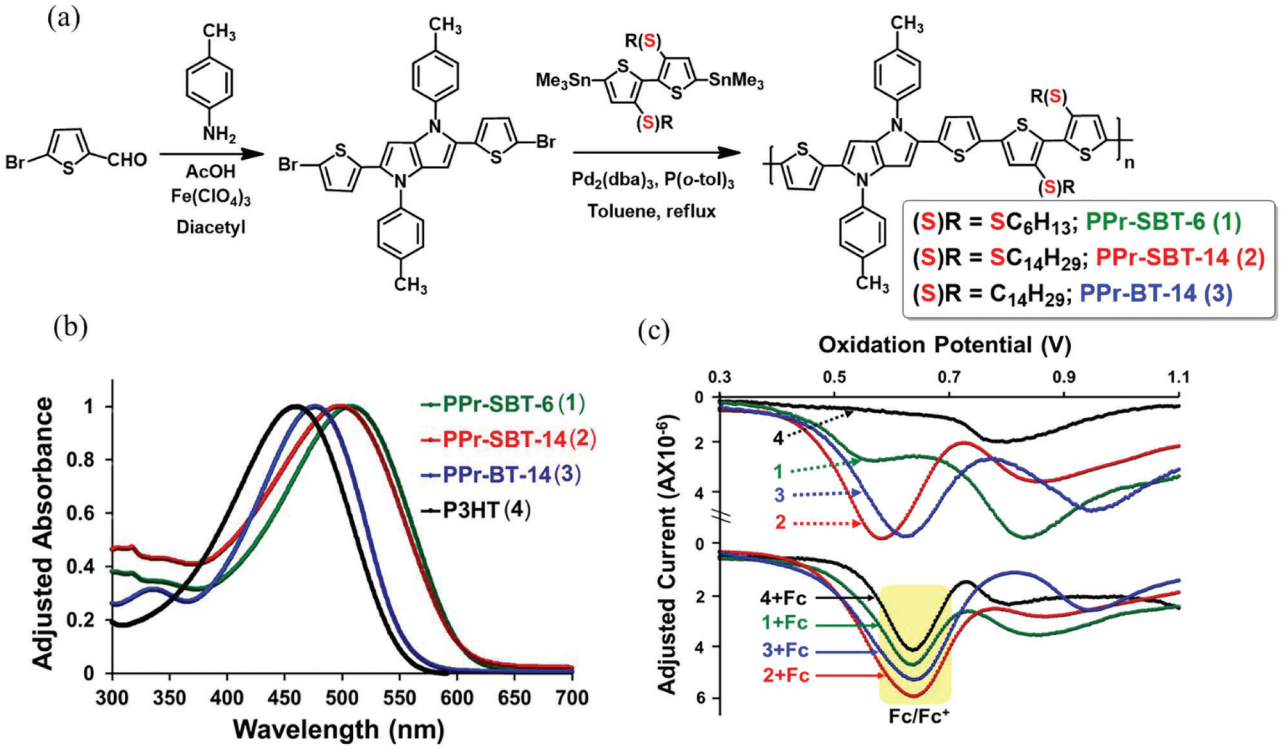

Figure 1. a) Scheme of synthetic route to the polymeric HTLs (**1–3**). b) Normalized UV–vis absorption spectra of all polymers in dichlorobenzene solution. c) Adjusted differential pulse voltammograms (DPV) of PPr-SBT-6 (green; **1**), PPr-SBT-14 (red; **2**), PPr-BT-14 (blue; **3**), and P3HT (black; **4**) recorded in o-$C_6H_4Cl_2$ with/without addition of ferrocene (as internal standard; calibrated at +0.64 V). The DPV of each polymer is adjusted for clarity.

charge-diffusion length and produces uniform perovskite films, leading to the best performance of the regular and inverted perovskite solar cells.[16,17] In addition to the PEDOT:PSS and PTAA aforementioned, the fused heteroaromatics with π conjugated systems (heteroacenes) have recently emerged as interesting fluorescent platforms and exhibit good charge transport and photoconductivity in optoelectronic applications.[18] Heteroanalogues such as anthracene, pyrene, pyrazine, thieno pyrazine, and other hydrocarbons as well as compounds possessing a thiophene or furan core were also reported.[19–21]

In the present study, we report the synthesis and characterizations of a set of new polymers containing two unique monomers, pyrrolopyrrole (PPr) and thioalkylated bithiophene (SBT), bearing different long alkyl chains, to serve as HTMs for TPSCs. To the best of our knowledge, very limited heteroacenes based on the pyrrole scaffold have been reported to date. Gryko et al. developed electron rich PPr heterobicyclic core to be used in the field of optoelectronics.[22,23] The main advantages of pyrrole-based heteroacenes over their analogs comprising thiophene and furan are: 1) pyrrole is a better electron-donor than thiophene and furan which can lead to improved p-type organic semiconductors and 2) the functionalization of nitrogen in pyrrole is feasible (in contrast to oxygen in furan or sulfur in thiophene), which enables the addition of various groups for controlling polarity and solubility of the polymer. For this reason, PPr has been shown to be an excellent building block for the design of low band-gap polymers with high hole conductivity as potential photovoltaic materials. The second monomer is SBT-bearing hexyl or tetradecyl chains. The importance of the SBT unit is the formation of the intramolecular S(alkyl)···S(thiophene) lock to enhance the π-conjugation, established as a very good core for organic thin-film transistor (OTFT) and dye-sensitized solar cell (DSSC) applications reported elsewhere.[24–26] The introduction of a long alkyl chain in SBT will substantially increase the solubility of polymers during film formation and strongly influences the structural conformation as well as the packing and intramolecular interaction.[27–29] With the combination of electron-donating PPr and planar SBT monomers, the newly developed polymers (PPr-SBT) are expected to give high hole mobility and excellent hole extraction for TPSCs. Further, the tetradecylated PPr-BT polymer was also prepared for comparison. Finally, the photovoltaic performances of the three new polymeric HTMs are compared with the commercially available polymer poly(3-hexylthiophene-2,5-diyl) (P3HT). Our results indicate that the PPr-SBT-14 device attained a PCE of 7.6% with great long-term stability for shelf-storage in a glovebox over 6000 h, a remarkable record for TPSCs.

2. Results and Discussion

2.1. Synthesis

The synthetic route for the target polymeric HTLs (**1–3**) is shown in **Figure 1**a. First, the brominated monomer of 2,5-bis(5-bromothiophen-2-yl)-1,4-di-*p*-tolyl-1,4-dihydropyrrolo [3,2-*b*]pyrrole was synthesized by the simple condensation of 2-bromothiophene-5-aldehyde with *p*-toluidine in the acidic

Table 1. Thermal, optical, and electrochemical properties of polymeric HTLs.

Polymers	T_d [°C][a)]	T_m [°C][b)]	λ_{abs} (soln)[c)] [nm]	E_{Ox} [V][e)]	HOMO [eV][f)]	LUMO [eV][g)]	ΔE_g [eV] [h)]	λ_{onset} (soln)[d)] [nm]
PPr-SBT-6 (1)	361	152	510	0.56	−5.00	−3.00	2.00	616
PPr-SBT-14 (2)	360	128	502	0.58	−5.02	−3.03	1.99	620
PPr-BT-14 (3)	398	150	480	0.628	−5.07	−2.90	2.17	575
P3HT (4)	–	–	461	0.80	−5.25	−3.03	2.22	558

[a)] By TGA; [b)] By melting-point apparatus; [c)] Absorption spectra were measured in *o*-$C_6H_4Cl_2$; [d)] Onset absorption; [e)] By DPV in *o*-$C_6H_4Cl_2$, E_{ox} = Oxidative potential; [f)] $E_{HOMO} = -(4.44+0.64+E_{ox})$; [g)] E_{LUMO} estimated from $E_{HOMO} + E_g$; [h)] Optical energy bandgap calculated by $1240/\lambda_{onset}$.

medium at 50 °C, followed by the addition of diacetyl, as the procedure has been reported elsewhere.[29] Then, the corresponding stannylated alkylated/thioakylated bithiophenes monomers were prepared from the respective precursors.[24] Finally, Pd-catalyzed Stille coupling reactions of brominated PPr and stannylated SBT/BT monomers under a nitrogen atmosphere yielded the target polymers. All three obtained polymers were purified by Soxhlet extraction and recrystallized from CH_2Cl_2, then thoroughly characterized by ^{1}H NMR and ^{13}C NMR spectroscopy (Figures S1–S8, Supporting Information). The extracted polymeric fractions are soluble in common organic solvents to make them accessible for solution-processed device fabrication.

2.2. Thermal, Optical, and Electrochemical Properties

The thermal properties of all the polymers were studied by using thermogravimetric analysis (TGA) recorded under a nitrogen atmosphere at a heating rate of 10 °C min^{-1}. From TGA (Figure S9a, Supporting Information), the high thermal decomposition temperature corresponding to 5% weight loss of all the polymers occurred at a temperature higher than 350 °C. The high thermal stability is attributed to rigid PPr and SBT/BT units present in the polymers. Thus, devices fabricated with these materials are expected to exhibit excellent thermal stability. The differential scanning calorimetry (DSC) measurements of PPr-SBT-14, PPr-BT-14, and PPr-SBT-6 were also carried out (Figure S9b, Supporting Information). This indicates that the polymers are sufficiently thermally stable and characterized by low crystallinity and high thermal stability in the film state.

The absorption spectra of all the polymers recorded in dichlorobenzene display an absorption maximum at around 500 nm (Figure 1b), and the relevant data are depicted in **Table 1**. The polymers that exhibited broad optical absorption in the range of 400–600 nm are mainly attributed to $\pi-\pi^*$ electronic transition. From this absorption, the BT(14) chain containing polymer shows blue–shifted absorption (480 nm) compared to SBT incorporated polymers due to the SBT with enhanced π-conjugation via strong intramolecular S(alkyl)•••S(thio) interactions, also known as intramolecular lock. Solid-state planarization causes an increase in the absorption of longer wavelengths which is consistent with our previous reports.[30] The lesser planar with a more twisted backbone of P3HT gives a blue shift in the absorption spectrum compared to those of the PPr-based polymers. This could be the reason for the planar–fused PPr inside the polymer increasing the π-conjugation for an absorption of longer wavelengths than that of P3HT with only alkylated thiophene units.

Differential pulse voltammograms (DPVs) of each polymer shown in Figure 1c were recorded in o-dichlorobenzene solution with Bu_4NPF_6 as a supporting electrolyte and their corresponding energy level diagrams are displayed in Figure S10 (Supporting Information). The oxidation potential was calibrated using ferrocene as an internal standard, which was set at +0.64 V. The HOMO energy level of the polymer to the normal hydrogen electrode is calculated by adding 4.44 eV to the oxidation potential.[31] The LUMO value of each polymer could be estimated by the addition of its HOMO level with the bandgap value, which was derived from the onset of the absorption spectrum of each polymer (Figure 1b). The first oxidation potential of SBT/BT PPr-based polymers (near +0.6 V) came from the PPr unit present in the polymers and the peaks were clearly merged with the internal standard ferrocene oxidative peak. The second oxidation peaks appeared around +0.8 V and correlated with P3HT, corresponding to the alkylated poly-thiophene units involved in all the polymers. The estimated HOMO/LUMO values of the four polymers are −5.00/−3.00 eV for PPr-SBT-6 (**1**), −5.02/−3.03 eV for PPr-SBT-14 (**2**), −5.07/−2.90 eV for PPr-BT-14 (**3**), and −5.25/−3.03 eV for P3HT (**4**). With the electron-donating PPr moiety, the HOMO energies of three PPr-based polymers (−5.0 to −5.07 eV) are higher than that of P3HT (−5.25 eV). The calculated HOMO energy levels are well aligned with the valence band energy level of tin perovskite which promotes an effective extraction and transportation of the holes from the perovskite active layer to the ITO substrate.

2.3. DFT Calculations

The effect of polymers' frontier molecular orbitals (HOMO and LUMO) and ground-state electron density distributions were investigated via density functional theory (DFT) calculations at the M062X/6-31G(d,p) level of theory using the Gaussian 09 program package. Two monomer units and two constitutional repeating units (PPr and SBT/BT with $n = 2$, i.e., dimers) with methyl groups as the substituents R (**Figure 2**) were used as model systems. For the ground state structures of the dimers, the electronic distributions of HOMOs are nearly delocalized on the whole molecular skeleton showing the electron richness of the entire moiety, while the electron distributions of the LUMOs are localized on the core building block, especially on the extended thiophene units The spatially separated HOMO and LUMO levels are in favor of hole extraction and transport. The same trend was observed for PPr-BT polymers (Figure S11, Supporting Information). The dimers of the SBT polymer clearly exhibit a more

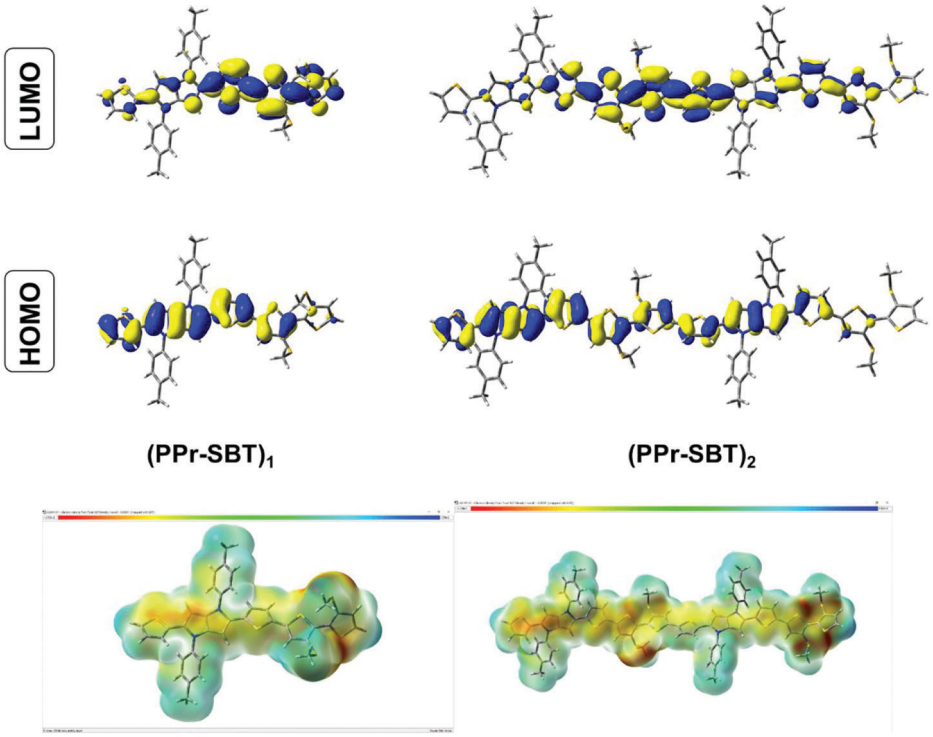

Figure 2. Optimized geometry of frontier molecular orbital diagrams for the model compounds and electrostatic surface potential (ESP) for PPr-SBT (with different combinations (PPr -SBT)$_1$ and (PPr- SBT)$_2$).

coplanar and rigid molecular conformation. As a result, the SBT polymers demonstrate better conjugation and tighter interchain stacking than the BT polymer, which results in higher mobility and a reduced energetic disorder. The electrostatic surface potential (ESP) map of PPr-SBT shows that the electron richness is mainly concentrated on the PPr core (Figure 2). The long chain substituted in the SBT unit increases the planarity which causes strong $\pi-\pi$ stacking and good solubility. Such kind of molecules are beneficial for perovskite's surface defect passivation and increase the stability of TPSCs. Furthermore, the excellent π-conjugation of the HOMO level, confirmed by the DFT calculations, ensures that the PPr-SBT polymers are suitable to serve as HTMs for TPSCs with great hole-extraction ability.

2.4. Morphology and Crystallinity Properties

The hydrophobicity of HTM could affect the morphology and crystallinity of the tin perovskite films.[24] Recent reports showed that it was difficult to cover the tin perovskite solution on HTMs with highly hydrophobic surfaces because of the fast crystallization of the tin perovskite.[13] The surface pretreatment with bulky organic salt, phenethylammonium iodide (PEAI), was successfully applied in PTAA to tune its surface hydrophobicity for high-performance TPSCs.[13] Although PEAI pretreatment can be used for PPr-SBT-14, we found another organic salt, anilinium iodide (ANI), yields superior device performance than over using PEAI, as the *J–V* results shown in Figure S12 (Supporting Information). For this reason, ANI was chosen for the pretreatment of polymeric HTM developed in this study.

The morphologies of the tin perovskite films fabricated on the polymeric HTMs were analyzed using atomic force microscopy (AFM) and scanning electron microscopy (SEM) techniques. The AFM images were obtained to study the surface properties of the different pristine HTMs and tin perovskites produced on these HTMs. The AFM images of HTMs with ANI pretreatment are shown in Figure S13 (Supporting Information). **Figure 3**a–d shows AFM images of tin perovskite films fabricated by two steps on a) PPr-SBT-14, b) PPr-SBT-6, c) PPr-BT-14, and d) P3HT, respectively, pretreated with ANI. It shows lower roughness and well-organization of tin perovskite on PPr-SBT-14 than on the others. SEM images of perovskite grains produced on PPr-SBT-14, PPr-SBT-6, PPr-BT-14, and P3HT are shown in Figure 3e–h, respectively. Apparently, tin perovskite produced on PPr-SBT-14 has larger and well-packed grains compared to the perovskites formed on other HTMs, which are consistent with the AFM images shown in Figure 3a–d. We deposited these polymeric HTMs onto the ITO substrates with and without ANI pretreatments and then measured the contact angles of the SnI_2 precursor on these HTMs for comparison. Not only the degree of polymerization but also the solution processability of the polymers affect device performance. Only the polymers with suitable solution processability exhibit the good device performance. Before pretreatment, as shown in Figure S14 (Supporting Information), the contact angles were 71.29°, 47.10°, 46.59°, and 36.16° for PPr-SBT-14, PPr-SBT-6, PPr-BT-14, and P3HT, respectively. PPr-SBT-14 has the largest contact angle due to its long alkyl side chain (as compared to PPr-SBT-6 and P3HT) and strong intramolecular S(alkyl)···S(thiophene) interaction (as compared to PPr-BT-14 and P3HT). After ANI modification,

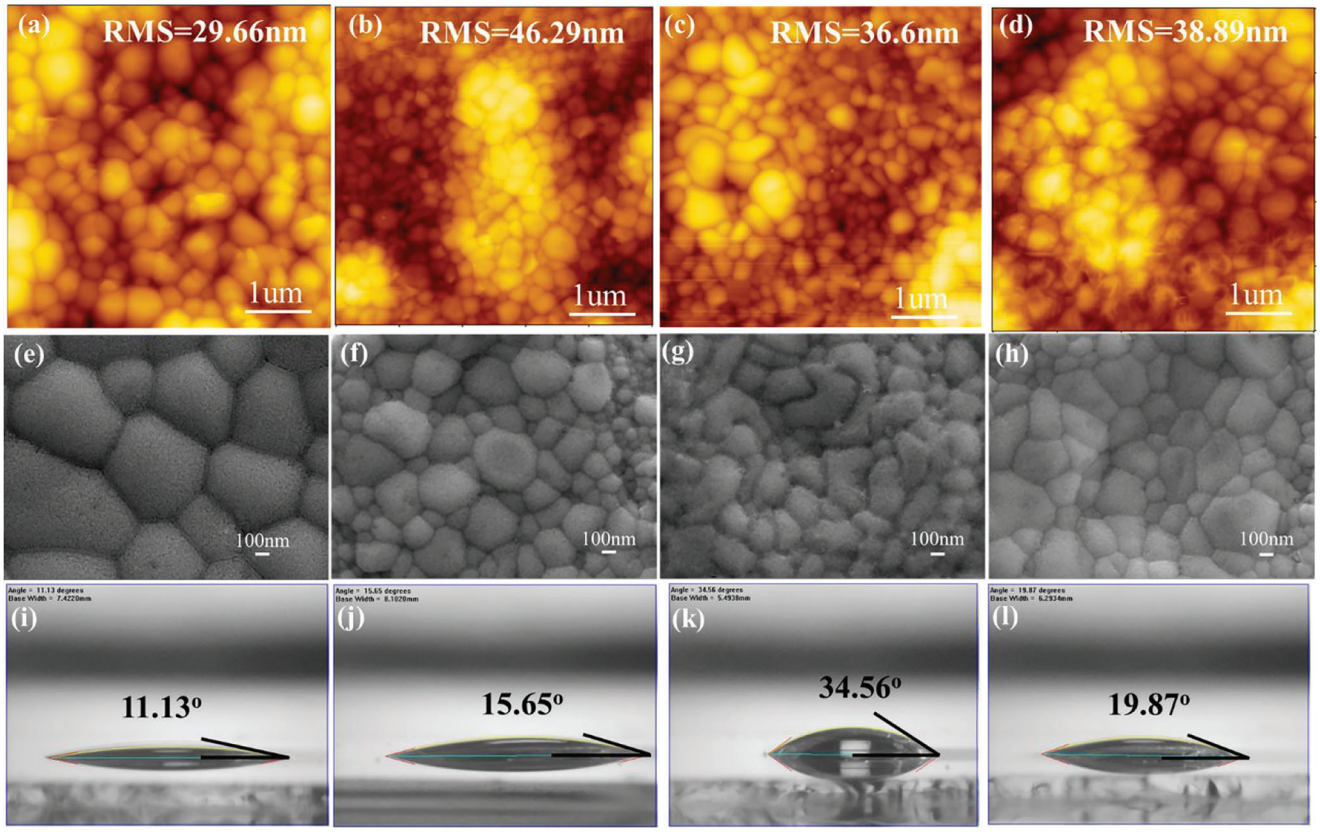

Figure 3. a–d) AFM images of tin perovskite made by two steps on PPr-SBT-14 (a), PPr-SBT-6 (b), PPr-BT-14 (c), and P3HT (d) surfaces. e–h) SEM images of tin perovskite fabricated on PPr-SBT-14 (e), PPr-SBT-6 (f), PPr-BT-14 (g), and P3HT (h) as HTMs. i–l) Contact angles of SnI_2 precursor solution deposited on PPr-SBT-14 I), PPr-SBT-6 (j), PPr-BT-14 (k), and P3HT (l).

contact angles on PPr-SBT-14, PPr-SBT-6, PPr-BT-14, and P3HT were significantly reduced to 11.13°, 15.65°, 34.56°, and 19.87° as shown in Figure 3i–l, respectively. If the contact angle of the precursor is too large, it is not beneficial for the crystallization of tin perovskite in the two-step method due to the serious surface tension effect. The photos shown in Figure S15a,b (Supporting Information) display the perovskite films fabricated on PPr-SBT-14 without and with ANI pretreatment, respectively. Uniform perovskite films cannot be produced without ANI modification. ANI, thus, has a significant effect on reducing the contact angle on the PPr-SBT-14 surface from 71.29° to 11.13°, feasible for the second step to deposit FAI on the SnI_2 surface and make a uniform tin perovskite film. The XRD patterns of tin perovskites produced on the four HTMs are shown Figure S16 (Supporting Information), where the perovskite on the PPr-BT-14 film gives the best crystallinity compared to others, in consistent with the high-resolution GIWAXS images at incident angle 0.02° shown in Figure S17 (Supporting Information) for all polymers. Therefore, we expect to observe good carrier transport and high PSC device performance for the PPr-SBT-14-based device.

2.5. Photovoltaic Properties and Characterizations

Figure 4a shows the *J–V* scan curves for the devices made of ANI-pretreated PPr-SBT-14, PPr-SBT-6, PPr-BT-14, and P3HT, according to a two-step fabrication procedure reported elsewhere.[13,14] P3HT was selected as a reference HTM to compare with the other PPr-based HTMs designed and synthesized in the present study. The TPSC based on P3HT attained a good performance with a PCE of 5.9%. For the PPr-based system, the PPr-SBT-14, PPr-SBT-6, and PPr-BT-14 devices attained the PCEs of 7.6%, 5.4%, and 4.9%, respectively; the corresponding photovoltaic parameters are listed in Table S1 (Supporting Information). The device performance shows a trend consistent with the morphology feature shown in Figure 3, i.e., the PPr-BT-14 device exhibits the poorest performance due to its poor morphology shown in Figure 3c (AFM) and Figure 3g (SEM). The PPr-SBT-14 device outperforms the reference P3HT device but the PPr-SBT-6 device showed poorer performance than the P3HT device. The long thioalkyl chains in PPr-SBT-14, thus, play an important role in increasing the hydrophobicity of the perovskite film to make uniform and well-packed crystal grains for enhanced device performance observed herein.

Figure 4b shows the IPCE spectra of the PPr-based devices with the calculated J_{SC} consistent with those shown in Figure 4a; the great performance of PPr-SBT-14 is due to its high J_{SC} value reflecting on the IPCE spectrum with an enhanced response in the spectral region of 350–650 nm, which is consistent with the absorption spectrum of PPr-SBT-14 shown in Figure 1b. Therefore, thicker PPr-SBT-14 film on the ITO substrate also had the effect of co-sensitization to contribute the photocurrents in the

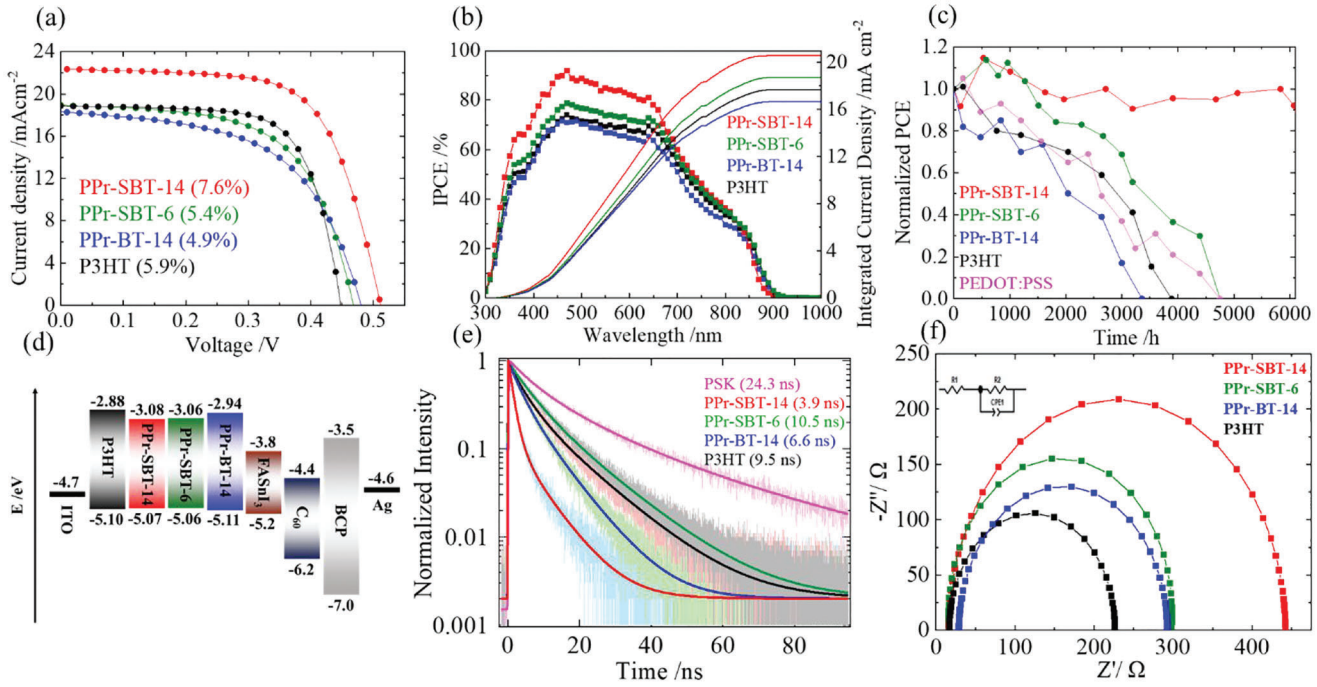

Figure 4. a) *J–V* characteristics, b) IPCE spectra, c) shelf stability of the devices, d) energy level diagram of each component, e) TCSPC PL decay profiles of tin perovskites on varied HTM, and f) EIS Nyquist plots for the devices or films made of tin perovskite deposited on varied PPr-based films or on P3HT as indicated.

visible absorption region. Such a co-sensitization effect was also observed on the PPr-SBT-6 film but to a smaller extent. Note that the film thicknesses of the HTMs are very small so that the absorption of HTM in front of perovskite films would not affect the light harvesting ability of tin perovskite in the 400–600 nm region, as the absorption spectra shown in Figure S18 (Supporting Information). The long-term stability data shown in Figure 4c is remarkable; for both P3HT and PPr-BT-14 devices, the performance degraded gradually to none around 3000–4000 h, similar to the device made of PEDOT:PSS. The PPr-SBT-6 device was stable within the initial 1500 h but gradually degraded to 40% of its initial value at 4000 h. In contrast, the PPr-SBT-14 device showed a remarkable long-term stability upon shelf storage in a glovebox with the PCE keeping constant at ≈100% for over 6000 h. Such a great stability on TPSCs has never been reported elsewhere.

Several factors are considered to explain the superior device performance and stability of the PPr-SBT-14 device. First, the contact angle of the precursor solution on the PPr-SBT-14 surface reduced significantly (Figure 3i) when ANI was treated for the HTM, which enhances the hydrophilicity of the film surface for rapid nucleation and thus produces the tin perovskite crystals with great sizes and uniformity as the SEM image shown in Figure 3e. The cross-sectional SEM images shown in Figure S19 (Supporting Information) confirm this point, for which the tin perovskite made on PPr-SBT-14 film gives the smoothest morphological feature among the others. Second, the energy level matching between HTM and tin perovskite is also an important factor to be considered. For this reason, we carried out ultraviolet photoelectron spectroscopy (UPS) measurements for each HTM (Figure S20, Supporting Information) to determine the valence band maximum (VBM) energy levels.[32] Using the bandgaps determined from the UV–vis spectra (Figure 1b and Table 1), the conduction band minimum (CBM) energy level values were determined for each species. Figure 4d shows the energy level diagram for all the HTMs together with other relevant species in the TPSC devices. The energy levels of HTMs determined by the UPS spectra for the thin-film samples are consistent with those determined by the DPV method for the solution samples (Figure S10, Supporting Information). Therefore, all the HTMs have suitable energy levels to match tin perovskite, as shown in Figure 4d, to give the appreciable device performance as shown in Figure 4a.

We also performed time-correlated single-photon-counting (TCSPC) measurements for the tin perovskite deposited on these HTMs; the corresponding PL decay profiles with excitation on the glass side are shown in Figure 4e, with the fitted decay coefficients listed in Table S2 (Supporting Information). We also measured TCSPC with excitation on the perovskite side; the corresponding PL decay profiles and fitted decay coefficients are shown in Figure S21 and Table S3 (Supporting Information), respectively. Because of surface defects, the perovskite-side excitation gives faster PL decays than the glass-side excitation, which is consistent with the results reported for lead perovskites.[33] Therefore, the discussions of hole-extraction abilities of these HTMs are based on the TCSPC results with the glass-side excitations. In the absence of HTM, the tin perovskite has a lifetime of 24.3 ns. When the HTMs were involved, the PL lifetimes decreased to reflect the effect of hole extraction from the perovskite to the HTM. The hole-extraction rates exhibit the trend with the order PPr-SBT-14 > PPr-BT-14 > P3HT > PPr-SBT-6, for which PPr-SBT-14 has the fastest hole-extraction rate. As a result, the J_{SC} of PPr-SBT-14 outperformed the others and gave the best

device performance among the others. Furthermore, electrochemical impedance spectral (EIS) studies examined the charge recombination property of PPr-based TPSCs compared with the P3HT device. The EIS measurements were performed in the dark with a bias voltage of 0.5 V. As shown in Figure 4f, only one semicircle appeared for all the Nyquist plots of the devices and it was fitted with an RC equivalent circuit model shown in the inset of Figure 4f. The fitted impedances represent the extent of charge recombination showing the order PPr-SBT-14 > PPr-SBT-6 > PPr-BT-14 > P3HT, which is consistent with the variation of V_{OC} showing a similar trend for these HTMs. Once again, the PPr-SBT-14 device has the largest charge recombination resistance to account for its greater V_{OC} over the others.

To understand the influence of charge carrier mobility on the photovoltaic performance, the hole mobilities of these HTMs thin film were measured by a space-charge limited current method and the corresponding results are shown in Figure S22 (Supporting Information). Due to the surface modification of the HTMs with ANI and the thinner HTM film characteristic, the obtained hole mobilities of these polymers are significantly greater than that of P3HT reported elsewhere.[34] The charge mobilities show the order PPr-SBT-14 > P3HT > PPr-BT-14 > PPr-SBT-6, a trend similar to that of the TCSPC results that account for the J_{SC} variation. Therefore, PPr-SBT-14 possessed all the excellent optoelectronic properties to stand out as the best HTM among all the others. To test the reproducibility, Figure S23 (Supporting Information) shows performance statistics (boxplots) of 40 devices with the raw data shown in Tables S4–S7 (Supporting Information). The effect of hysteresis was also tested for the PPr-SBT-14 device as the forward and reverse *J–V* scans shown in Figure S24 (Supporting Information). Furthermore, the performances of the fresh PPr-SBT-14 and PEDOT:PSS devices were measured under one sun illumination at the maximum-power point (MPP) in ambient air conditions (≈50% RH) as the results shown in Figure S25 (Supporting Information). The MPP measurements indicate the intrinsic light-soaking stability of an unencapsulated PPr-SBT-14 device lasting for 5 h, for which the PCE of the PEDOT:PSS device degraded to 60% of its original performance in 5 h (Figure S25, Supporting Information). This study thus reveals a new class of PPr-SBT conducting polymers serving as HTMs for TPSCs with outstanding stability on shelf-storage in dark and under light-soaking condition without encapsulation.

3. Conclusions

Traditionally PEDOT:PSS was used to fabricate a tin perovskite ($FASnI_3$) solar cell according to a one-step procedure. However, since the reaction between SnI_2 and FAI is very rapid, other hole-transporting materials with high hydrophobicity do not work for TPSCs using the traditional method. Herein, we design and synthesize three thioalkylated/alkylated bithiophene incorporated pyrrolopyrrole-based polymers as HTMs for TPSCs. The reported polymeric HTMs are quite hydrophobic so good device stability is expected. To overcome the film formation problem aforementioned, we treated the HTMs with ANI additive to improve the hydrophilicity of the HTM film and fabricated the tin perovskite layer using a two-step approach. This approach was very successful and made PPr-SBT-14 the superior device to attain a PCE of 7.6% with a shelf-storage stability over 6000 h without encapsulating the device. The PPr-SBT-14 device thus becomes a model system for the development of other hydrophobic HTMs for TPSC with great performance and stability.

Supporting Information

Supporting Information is available from the Wiley Online Library or from the author.

Acknowledgements

C.-H.K. and R.B. contributed equally to this work. The authors thank Dr. Y.-W. Tsai and Dr. J.-M. Lin (TPS 25A1, NSRRC) for their kind assistance in GI-WAXS data analysis. M.-C.C. thanks the financial support provided by the Ministry of Science and Technology (MOST) of Taiwan (MOST 111-2113-M-008 -004 -MY3) and NCU-Covestro Research Center (NSTC 111-2622-8-008-006). E.W.-G.D. thanks the support by National Science and Technology Council (NSTC), Taiwan (grant No. NSTC 111-2634-F-A49-007, NSTC 111-2123-M-A49-001) and the Center for Emergent Functional Matter Science of National Yang Ming Chiao Tung University (NYCU) from The Featured Areas Research Center Program within the framework of the Higher Education Sprout Project by the Ministry of Education (MOE) in Taiwan. J.-S.N. thanks the Ministry of Science and Technology (Grant No. MOST 109-2113-M-992-001-MY2) for financial support.

Conflict of Interest

The authors declare no conflict of interest.

Data Availability Statement

The data that support the findings of this study are available from the corresponding author upon reasonable request.

Keywords

polymeric hole-transport materials, pyrrolopyrrole, thioalkylated bithiophene, tin perovskite solar cells

Received: January 21, 2023
Revised: April 1, 2023
Published online:

[1] S. N. Afraj, D. Zheng, A. Velusamy, W. Ke, S. Cuthriell, X. Zhang, Y. Chen, C. Lin, J.-S. Ni, M. R. Wasielewski, *ACS Energy Lett.* **2022**, *7*, 2118.
[2] E. W.-G. Diau, *ACS Energy Lett.* **2017**, *2*, 334.
[3] S. N. Afraj, A. Velusamy, C.-Y. Chen, J.-S. Ni, Y. Ezhumalai, C.-H. Pan, K.-Y. Chen, S.-L. Yau, C.-L. Liu, C.-H. Chiang, *J. Mater. Chem. A* **2022**, *10*, 11254.
[4] T.-W. Chen, S. N. Afraj, S.-H. Hong, L.-H. Chou, A. Velusamy, C.-Y. Chen, Y. Ezhumalai, S.-H. Yang, I. Osaka, X.-F. Wang, *ACS Appl. Energy Mater.* **2022**, *5*, 4149.
[5] E. W.-G. Diau, E. Jokar, M. Rameez, *ACS Energy Lett.* **2019**, *4*, 1930.
[6] X. Chen, Z. Jia, Z. Chen, T. Jiang, L. Bai, F. Tao, J. Chen, X. Chen, T. Liu, X. Xu, *Joule* **2020**, *4*, 1594.
[7] W. Ma, T. Jiang, Z. Yang, H. Zhang, Y. Su, Z. Chen, X. Chen, Y. Ma, W. Zhu, X. Yu, *Adv. Sci.* **2021**, *8*, 2003728.

[8] W. Ma, Y. Su, Q. Zhang, C. Deng, L. Pasquali, W. Zhu, Y. Tian, P. Ran, Z. Chen, G. Yang, *Nat. Mater.* **2022**, *21*, 210.
[9] F. Zhang, H. Lu, J. Tong, J. J. Berry, M. C. Beard, K. Zhu, *Energy Environ. Sci.* **2020**, *13*, 1154.
[10] S. Toda, E. W.-G. Diau, S. Shigeto, *J. Phys. Chem. C* **2021**, *125*, 27996.
[11] B. B. Yu, Z. Chen, Y. Zhu, Y. Wang, B. Han, G. Chen, X. Zhang, Z. Du, Z. He, *Adv. Mater.* **2021**, *33*, 2102055.
[12] X. Jiang, H. Li, Q. Zhou, Q. Wei, M. Wei, L. Jiang, Z. Wang, Z. Peng, F. Wang, Z. Zang, *J. Am. Chem. Soc.* **2021**, *143*, 10970.
[13] C.-H. Kuan, G.-S. Luo, S. Narra, S. Maity, H. Hiramatsu, Y.-W. Tsai, J.-M. Lin, C.-H. Hou, J.-J. Shyue, E. W.-G. Diau, *Chem. Eng. J.* **2022**, *450*, 138037.
[14] S. Shahbazi, M.-Y. Li, A. Fathi, E. W.-G. Diau, *ACS Energy Lett.* **2020**, *5*, 2508.
[15] D. Song, S. Narra, M.-Y. Li, J.-S. Lin, E. W.-G. Diau, *ACS Energy Lett.* **2021**, *6*, 4179.
[16] Q. Jiang, J. Tong, Y. Xian, R. A. Kerner, S. P. Dunfield, C. Xiao, R. A. Scheidt, D. Kuciauskas, X. Wang, M. P. Hautzinger, *Nature* **2022**, *611*, 278.
[17] Q. Jiang, J. Tong, R. A. Scheidt, X. Wang, A. E. Louks, Y. Xian, R. Tirawat, A. F. Palmstrom, M. P. Hautzinger, S. P. Harvey, *Science* **2022**, *378*, 1295.
[18] A. Velusamy, S. N. Afraj, S. Yau, C. L. Liu, Y. Ezhumalai, P. Kumaresan, M. C. Chen, *J. Chin. Chem. Soc.* **2022**, *69*, 1253.
[19] H. Guo, H. Zhang, S. Liu, D. Zhang, Y. Wu, W.-H. Zhu, *ACS Appl. Mater. Interfaces* **2022**, *14*, 6852.
[20] J. Qiu, H. Liu, X. Li, S. Wang, *Chem. Eng. J.* **2020**, *387*, 123965.
[21] L. Gao, T. H. Schloemer, F. Zhang, X. Chen, C. Xiao, K. Zhu, A. Sellinger, *ACS Appl. Energy Mater.* **2020**, *3*, 4492.
[22] B. Sadowski, K. Hassanein, B. Ventura, D. T. Gryko, *Org. Lett.* **2018**, *20*, 3183.
[23] M. Tasior, B. Koszarna, D. C. Young, B. Bernard, D. Jacquemin, D. Gryko, D. T. Gryko, *Org. Chem. Front.* **2019**, *6*, 2939.
[24] S. Vegiraju, B. C. Chang, P. Priyanka, D. Y. Huang, K. Y. Wu, L. H. Li, W. C. Chang, Y. Y. Lai, S. H. Hong, B. C. Yu, *Adv. Mater.* **2017**, *29*, 1702414.
[25] Y. Ezhumalai, F.-S. Lin, M.-S. Fan, K. Prabakaran, J.-S. Ni, Y.-C. Wu, G.-H. Lee, M.-C. Chen, K.-C. Ho, *ACS Appl. Mater. Interfaces* **2020**, *12*, 15071.
[26] S. N. Afraj, C. C. Lin, A. Velusamy, C. H. Cho, H. Y. Liu, J. Chen, G. H. Lee, J. C. Fu, J. S. Ni, S. H. Tung, *Adv. Funct. Mater.* **2022**, *32*, 2200880.
[27] H. Chen, Y. Guo, G. Yu, Y. Zhao, J. Zhang, D. Gao, H. Liu, Y. Liu, *Adv. Mater.* **2012**, *24*, 4618.
[28] C. Wang, Y. Qin, Y. Sun, Y.-S. Guan, W. Xu, D. Zhu, *ACS Appl. Mater. Interfaces* **2015**, *7*, 15978.
[29] H. Huang, L. Yang, A. Facchetti, T. J. Marks, *Chem. Rev.* **2017**, *117*, 10291.
[30] Y. Liu, Z. Zhang, S. Feng, M. Li, L. Wu, R. Hou, X. Xu, X. Chen, Z. Bo, *J. Am. Chem. Soc.* **2017**, *139*, 3356.
[31] E. Jokar, H.-S. Chuang, C.-H. Kuan, H.-P. Wu, C.-H. Hou, J.-J. Shyue, E. Wei-Guang Diau, *J. Phys. Chem. Lett.* **2021**, *12*, 10106.
[32] C.-C. Chueh, C.-Z. Li, A. K.-Y. Jen, *Energy Environ. Sci.* **2015**, *8*, 1160.
[33] W. Chen, B. Han, Q. Hu, M. Gu, Y. Zhu, W. Yang, Y. Zhou, D. Luo, F.-Z. Liu, R. Cheng, *Sci. Bull.* **2021**, *66*, 991.
[34] H. Sirringhaus, N. Tessler, R. H. Friend, *Science* **1998**, *280*, 1741.